Developmental Biology 332 (2009) 287–298

Contents lists available at ScienceDirect

Developmental Biology

journal homepage: www.elsevier.com/developmentalbiology

Lmx1b is essential for survival of periocular mesenchymal cells and influences Fgf-mediated retinal patterning in zebrafish

Carrie McMahon [a,1], Gaia Gestri [b,1], Stephen W. Wilson [b], Brian A. Link [a,*]

[a] Department of Cell Biology, Neurobiology, and Anatomy, Medical College of Wisconsin, 8701 Watertown Plank Road, BSB 431, Milwaukee, WI 53226, USA
[b] Department of Cell and Developmental Biology, UCL, Gower Street, London 6BT WC1, UK

ARTICLE INFO

Article history:
Received for publication 7 January 2009
Revised 27 April 2009
Accepted 29 May 2009
Available online 3 June 2009

Keywords:
lmx1b.1
lmx1b.2
Coloboma
Glaucoma
Periocular mesenchyme
Ocular morphogenesis
Zebrafish

ABSTRACT

To gain insight into the mechanisms of Lmx1b function during ocular morphogenesis, we have studied the roles of *lmx1b.1* and *lmx1b.2* during zebrafish eye development. In situ hybridization and characterization of transgenic lines in which GFP is expressed under *lmx1b.1* regulatory sequence show that these genes are expressed in periocular tissues and in a pattern conserved with other vertebrates. Anti-sense morpholinos against *lmx1b.1* and *lmx1b.2* result in defective migration of periocular mesenchymal cells around the eye and lead to apoptosis of these cells. These defects in the periocular mesenchyme are correlated with a failure in fusion of the choroid fissure or in some instances, more severe ventral optic cup morphogenesis phenotypes. Indeed, by blocking the death of the periocular mesenchyme in Lmx1b morphants, optic vesicle morphogenesis is largely restored. Within the retina of *lmx1b* morphants, Fgf activity is transiently up-regulated and these morphants show defective naso-temporal patterning. Epistasis experiments indicate that the increase in Fgf activity is partially responsible for the ocular anomalies caused by loss of Lmx1b function. Overall, we propose zebrafish *lmx1b.1* and *lmx1b.2* promote the survival of periocular mesenchymal cells that influence multiple signaling events required for proper ocular development.

Introduction

During eye development, the optic vesicles evaginate from the forebrain neuroepithelium and come into contact with several other tissues that are required for correct ocular morphogenesis, patterning and differentiation. For instance, contact with the prospective lens epithelium is correlated with invagination of the optic vesicle to form the two-layered optic cup consisting of prospective neural retina and pigment epithelium. Several recent studies have suggested that periocular mesenchyme derived from head mesoderm and neural crest cells also plays roles in the early morphogenesis of the optic cup and differentiation of the retina (Fuhrmann et al., 2000; Matt et al., 2005; Lupo et al., 2005; Molotkov et al., 2006; Matt et al. 2008).

Periocular mesenchyme eventually gives rise to specialized structures of the anterior segment of the eye that are responsible for aqueous humor dynamics (Johnston et al., 1979; Trainor & Tam, 1995; Cvekl and Tamm, 2004; Gage et al., 2005). Consequently, in humans disruption to factors important for the survival, migration and/or differentiation of periocular mesenchymal cells can lead to dysgenesis of the ocular anterior segment, elevated intraocular pressure and increased risk of glaucoma (Gould et al., 2004).

The glaucomas are a group of complex diseases characterized by vision loss due to damage of the optic nerve. Progress has been made towards identification of a subset of the critical risk genes for glaucoma. Several of these are also essential for ocular anterior segment development. Examples include genes encoding the transcription factors *PITX2*, *FOXC1*, and *LMX1B*. Mutations in either *PITX2* or *FOXC1* result in Axenfield–Reiger syndrome, in which a subset of affected individuals develop glaucoma (Walter, 2003). The roles of *PITX2* and *FOXC1* in eye development have been explored in several species (Nishimura et al., 1998; Mears et al., 1998; Kidson et al., 1999; Smith et al. 2000; Semina et al., 1996; Gage et al., 1999; Tamimi et al., 2006). However, the role of *LMX1B* during ocular morphogenesis is less well understood.

LMX1B encodes a LIM-homeodomain transcription factor that when mutated in humans causes Nail-Patella Syndrome (NPS), a pleiotropic condition where approximately 50% of patients develop elevated IOP and glaucoma (Dreyer et al., 1998; Vollrath et al., 1998). In addition to the eye, NPS affects joint and limb development, and often disrupts function of the renal and central nervous systems (CNS). Genetic and biochemical analyses have shown that NPS is due to *LMX1B* haploinsufficiency (Lichter et al., 1997; Vollrath et al., 1998). Unlike NPS patients that are heterozygous for *LMX1B* mutations, mice heterozygous for null mutations appear normal. However, homozygous mutant mice display several abnormalities observed in NPS patients including abnormal development of renal structures, CNS patterning defects and dysgenesis of anterior ocular tissues (Chen et al., 1998; Kania et al., 2000; Guo et al., 2007;

* Corresponding author. Fax: +1 414 456 6517.
E-mail address: blink@mcw.edu (B.A. Link).
[1] These authors gave equal contribution and are considered co-first authors.

0012-1606/$ – see front matter © 2009 Elsevier Inc. All rights reserved.
doi:10.1016/j.ydbio.2009.05.577

Pressman et al., 2000). However, it remains unknown how LMX1B regulates ocular development.

To better understand the mechanisms by which Lmx1b defects cause ocular pathology, we examined the expression and loss-of-function phenotypes of *lmx1b.1* and *lmx1b.2* in zebrafish. Analysis revealed that both genes have expression patterns conserved with other vertebrates, including within the periocular mesenchyme. Loss-of-function analyses showed Lmx1b activity is required for periocular mesenchymal cell survival, optic cup morphogenesis and choroid fissure closure. In addition, knock-down of Lmx1b in transgenic lines that express GFP under *lmx1b.1* regulatory sequence revealed migration defects in periocular mesenchyme. We also found that *lmx1b* morphants showed increased ocular FGF activity, and consistent with this, abnormal naso-temporal patterning of the retina (Picker and Brand, 2005). Preventing apoptosis of periocular mesenchyme in *lmx1b* morphants alleviated the morphogenesis defects. Furthermore, reducing Fgf activity partially restored retinal patterning. Together, these results suggest that altered Fgf signaling due to periocular mesenchymal cell death is a contributing factor to the ocular pathogeneses associated with loss of Lmx1b activity.

Materials and methods

Animals

Zebrafish embryos were raised at 28.5 °C and staged according to Kimmel et al. (1995). Phenylthiourea (PTU) was applied to embryos to prevent melanization when necessary.

Transgenic and mutant lines

Tg(*h2afx*:H2A-mCherry)^{mw3} (this study)
Tg(−5 kb*lmx1b.1*:GFP)^{mw10,11,12,13} (this study)
Tg(*foxd3*:GFP)^{zf15} (Gilmour et al. 2002)
Tg(−7.2*sox10*:EGFP)^{zf77} (Hoffman et al., 2007)
Tg(fli1a:EGFP)^{y5} (Lawson and Weinstein, 2002)
Tg(*dusp6*:EGFP)^{pt6} (Molina et al., 2007)
Tg(*Bactin*:HRAS-EGFP)^{vu119} (Cooper et al., 2005)
fgf8a^{ti282} (*acerebellar*) (Reifers et al., 1998).

Isolation of full-length lmx1b.1 and lmx1b.2 cDNA

Total RNA was extracted from adult zebrafish eyes using RNAeasy Mini Kit (Qiagen). RT-PCR combined with 5′ and 3′ RACE was performed to identify full-length *lmx1b.1*. To isolate *lmx1b.1* full-length sequence, the following primers were used:

*lmx1b.1*flF 5′ATGTTGGACGGTATAAAAATCGAA
*lmx1b.1*flR 5′TCATGAGGCGAAATAGGAGCTC.

Full-length *lmx1b.2* sequence was isolated by RT-PCR using the following primers:

*lmx1b.2*flF 5′AGTAGACATGCTGGACGGAAT
*lmx1b.2*flR 5′GAGCTCCTACTTCACCTCCTGA.

Accession tags

Zebrafish *lmxb.1* (AY551077) and *lmx1b.2* (AY551078) sequences have been deposited into GenBank.

Histology

Embryos were dechorionated and fixed overnight at 4 °C in 2.5% gluteraldehyde/1% paraformaldehyde in phosphate-buffered sucrose, pH7.4. The next morning embryos were dehydrated and infused with Epon. Transverse sections were 1 μm thick, heat-mounted on gelatin coated glass slides, and stained with 1% toluidine blue.

In situ hybridization

Whole mount in situ hybridization was performed as previously described (Thisse and Thisse, 2004) with one modification. Following LiCl precipitation, anti-sense RNA probe was further purified using a ProbeQuant G-50 micro spin column (GE Healthcare).

Morpholino oligonucleotides

Morpholino oligonucleotides (GeneTools, Inc.) were targeted to splice site junctions between exon 1 and intron 1 (splice-MOs) and the translation start site (ATG-MOs) for each *lmx1b.1* or *lmx1b.2*. The following morpholino sequences were used:

lmx1b.1—ATG, 5′CTTCGATTTTTATACCGTCCAACAT (O'Hara et al., 2005)
lmx1b.2—ATG, 5′GATTCCGTCCAGCATGTCTACTTGA
lmx1b.1—splice, 5′TTGAAGGACTTACCGAGCATAACTC
lmx1b.2—splice 5′GTGTGTGTGAAACTCACCCAGCATC.

Mismatch controls had sequences matching those of the splice-inhibiting morpholinos with the exception of 5 bases denoted in lowercase letters:

5 mismatch *lmx1b.1*—splice 5′TTcAAcGACTTAgCGAGgATAAgTC
5 mismatch *lmx1b.2*—splice 5′GTcTGTcTGAAAgTCACCgAGgATC.

For each *lmx1b* gene, translation-inhibiting and pre-mRNA splice-inhibiting morpholinos were injected at the one-cell stage with 1% phenol red (Nasevicius and Ekker, 2000). For *lmx1b.1* and *lmx1b.2*, both translation- and splice-inhibiting morpholinos produced similar phenotypes. As controls, morpholinos with 5 base-pairs mismatched relative to the splice-disrupting oligos did not produce phenotypes when injected at similar concentrations to those used for the experimental morpholinos. Each splice-disrupting morpholino inhibited normal transcript processing while mismatch control morpholinos did not. Quantitative real-time RT-PCR determined that the *lmx1b* splice-inhibiting morpholinos functioned as predicted. For *lmx1b* morphant experiments described in the Results section, splice-inhibiting morpholinos were used and for most analyses, embryos showing moderate phenotypes were analyzed (see Fig. 2 and Table S1 for details).

Additional morpholinos were used as previously published:

fgf8a MO 5′TGAGTCTCATGTTTATAGCCTCAGT3′ (Albertson and Yelick, 2005)
fgf3 MO2 5′GGTCCCATCAAAGAAGTATCATTTG3′ (Maves et al., 2002)
fgf3 MO3 5′TCTCGCTGGAATAGAAAGAGCTGGC3′ (Maves et al., 2002)
p53 MO 5′GCGCCATTGCTTTGCAAGAATTG (Robu et al., 2007).

Lmx1b.1 promoter and cDNA expression constructs

RT-PCR was used to isolate −5 kb of the *lmx1b.1* promoter using the following primers designed from HTG sequence clone CH211-81G2:

Lmx1b.1–5 kb F 5′GGGGACAACTTTGTATAGAAAAGTTGA-TCACGTGCTTTTGGGTTTC and Lmx1b.1–5 kb R 5′GGGGACTGCCTT-TTTTGTACAAACTTGGCGGATGATCTTCGATTTT. Gateway technology (Invitrogen) using Tol2-kit reagents (Kwan et al. 2007) was employed to generate tol2:−5*lmx1b.1*:lmx1b:ires:GFP and tol2:−5*lmx1b.1*:GFP. Expression of the tol2 constructs was achieved by co-injection of transposase mRNA as previously described (Kawakami 2005).

Quantitative real-time RT-PCR

Two independent sets each of 18 somite stage and 24 h post fertilization (hpf) embryos, each analyzed in triplicate, injected with either *lmx1b.1*, *lmx1b.2*, or *lmx1b.1*+*lmx1b.2* (*lmx1b*dMO) splice-inhibiting morpholinos were collected for total RNA isolation using the QIAGEN RNeasy Plus Mini Kit (QIAGEN Inc.). Age-matched uninjected embryos were collected and RNA was isolated in parallel with morphant RNA. The degree of gene knock-down was evaluated as the average fold-reduction as compared to age-matched uninjected embryos. cDNA was produced using 0.5 μg of RNA with the SuperScript II Reverse Transcriptase enzyme (Invitrogen). qPCR reactions were carried out using the iQ SYBR Green Supermix (Bio-Rad) on the iCycler iQ Real-Time Detection System (Bio-Rad). All cDNA samples were assayed in triplicate for each primer set. Primers to amplify a 240 base pair (bp) fragment of *lmx1b.1* were designed (F: 5′-TTGGACGGTATAAAAATCGAAGA-3′; R: 5′-TTTG-CAGTAAAGTTTCCTCTCC-3′). Primers to amplify a 249 bp fragment of *lmx1b.2* were designed (F: 5′-ATGCTGGACGGAATCAAAATT-3′; R: 5′-AGTCGTGTTTACAGTAGAGTTTGTGG-3′). Amplification of *ef1-alpha* was used for normalization (F: 5′-TGGGCACTCTACTTAAGGAC-3′; R: 5′-TGTGCCAACAGGTGCAGTTC-3′).

TUNEL analysis

TUNEL labeling to detect apoptosis was performed using the Apoptag kit (Chemicon International). The manufacturer's instructions were followed for the labeling reaction and embryos were then washed in phosphate-buffered saline, blocked and developed as described for a standard whole mount in situ hybridization/antibody labeling protocol (Shanmugalingam et al., 2000).

Immunocytochemistry

Antibodies to activated Caspase-3 (affinity purified rabbit polyclonal, R&D Systems Cat #AF835, Lot#CFZ32) and phospho(ser10) Histone-H3 (rabbit polyclonal, Upstate—Millipore Cat#06-570, Lot#28770) were both used on 4% paraformaldehyde-fixed cryosections at 1:1000 dilution.

Ffg-receptor inhibitor treatment

The Ffg-receptor inhibitor SU5402 (Calbiochem) was stored as 10 mM stock solutions in DMSO and added to 6 somite stage embryos at a final concentration of 5 μM. Control embryos were treated with DMSO at equivalent concentrations.

Genetic mosaics

Blastulae transplantation was performed as previously described to generate chimeric embryos (Ho and Kane, 1990). Embryos derived from matings of Tg(*foxd3*:GFP)^{zf15} and Tg(*h2afx*:H2A-mCherry)^{mw3} were used as donors. Approximately equivalent numbers of cells (~20–25 cells) were transplanted in wild-type unlabeled hosts after the 1000 cell stage and before the dome-stage. Following the transplantation of blastulae cells into the ventral blastoderm margin, a region fated for neural crest, mosaic embryos were raised to 30 hpf. At 30 hpf, mosaic embryos were screened for at least 1 mCherry-positive nuclei in the ocular mesenchyme to indicate that neural crest targeting was achieved, and these specimens were fixed in 4% paraformaldehyde for quantitative analysis. Wild-type and *lmx1b*dMO donor mosaics were scored for the number of H2A-mCherry and *foxD3*:GFP-positive cells using a compound fluorescent microscope. Two separate experiments were carried out to achieve an $n = 12$ embryos for each condition. A third experiment was carried out to compare mismatch *lmx1b*dMO donor cell behavior to that of uninjected wild-type donor cells. No differences were noted between these two control donor cell types.

Results

Zebrafish lmx1b.1 and lmx1b.2 are expressed in ocular and non-ocular tissues

Transcripts for *lmx1b.1* and *lmx1b.2* are expressed dynamically and largely in overlapping domains during embryonic development (Fig. 1). Before the 13 somite stage(s), both genes were expressed in the prospective midbrain–hindbrain boundary (MHB) and axial midline tissue (O'Hara et al., 2005). At 18 s, both *lmx1b.1* and *lmx1b.2* were expressed in the MHB, ventral diencephalon, and midline tissues (Figs. 1A, G) and at 24 and 36 hpf, in the ventral diencephalon, midline, fin buds, nephric primordia, MHB and hindbrain cells (Figs. 1B–E; H–K). We observed unique expression of *lmx1b.1* in the dorsal diencephalon and otic vesicles at 18 s (Fig. 1A), and in spinal cord cells (Figs. 1B, E boxed). By 42 hpf, *lmx1b.1* expression was maintained in diencephalic, midbrain and hindbrain cells, and fins (Fig. 1F). *lmx1b.2* transcripts were detected in domains overlapping with *lmx1b.1*, but expression was more restricted (Figs. 1H–L). Indeed, the expression domains of *lmx1b.1* were broader than those of *lmx1b.2* throughout all developmental stages analyzed.

Within the ocular region, transcripts for both *lmx1b* genes were detected in periocular cells associated with the optic stalk (Figs. 1C, I)

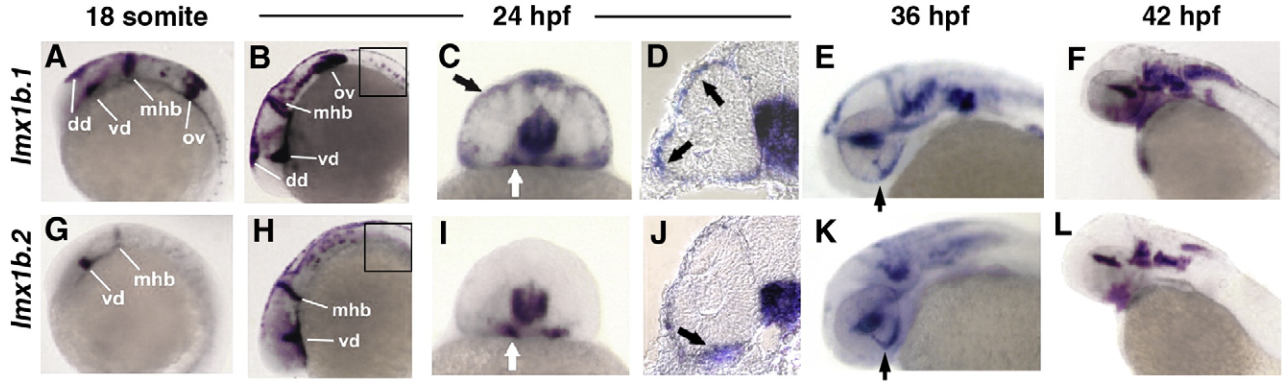

Fig. 1. Zebrafish *lmx1b.1* and *lmx1b.2* are expressed in the ocular and non-ocular tissue. *In situ* hybridization of *lmx1b.1* (A–F) and *lmx1b.2* (G–L) from 18 s to 42 hpf. Anterior is to the left in lateral views. Expression of both *lmx1b* genes was strong in the midbrain–hindbrain boundary and ventral diencephalon at 18 s (A, G) and 24 hpf (B, H). Only *lmx1b.1* was detected in the otic vesicle (A versus G) and spinal cord neurons (B versus H, boxed). For both genes, periocular expression in cells associated with the optic stalk (white arrows C, I) and the globe of the eye (black arrows C, I), was observed in whole mount and histological sections (arrows D, J). Expression of *lmx1b.1* and *lmx1b.2* was also detected in the ventral fissure (arrows E, K) and hindbrain neurons (E, F and K, L). See text for additional details. mhb, midbrain–hindbrain boundary; vd, ventral diencephalon; dd, dorsal diencephalon; ov, otic vesicle; hb, hindbrain.

and periocular mesenchyme underlying the surface ectoderm at 24 hpf (Figs. 1D, J). By 36 hpf, *lmx1b.1* expression persisted in periocular mesenchyme and was enriched in presumptive anterior segment structures and cells of the optic fissure (Figs. 1E, K). By 42 hpf, *lmx1b.1* expression was also associated with the hyaloid vasculature (data not shown). Similar to *lmx1b.1*, *lmx1b.2* was expressed in periocular mesenchyme at 24 hpf, and in cells lining the optic fissure by 36 hpf (Figs. 1I–K).

Overall, the expression patterns of the duplicated *lmx1b* genes were overlapping and highly conserved when compared with those of higher vertebrate orthologues (Dunston et al., 2005). Overlapping expression patterns suggest at least partial redundancy of function and previous studies have indeed shown that *lmx1b.1* and *lmx1b.2* have redundant functions in maintaining the isthmic organizer (O'Hara et al., 2005).

Abrogation of lmx1b.1 and lmx1b.2 function results in severe eye morphogenesis defects

To explore the role of *lmx1b.1* and *lmx1b.2* in eye development, anti-sense morpholinos were used to diminish their function. For each *lmx1b* gene, translation-inhibiting and pre-mRNA splice-inhibiting morpholinos were tested. Both types of morpholinos produced CNS phenotypes as previously observed (O'Hara et al., 2005; Filippi et al., 2007); however, the splicing morpholinos were more efficient and were used for our analyses (see Materials and methods, Supplemental Fig. S1, and Table S1 for details).

By 24 hpf, embryos injected with either *lmx1b.1* or *lmx1b.2* morpholinos showed defects in ventral eye morphogenesis. Co-injection of *lmx1b.1* and *lmx1b.2* morpholinos, herein referred to as *lmx1b*dMO morphants, typically resulted in more severe ocular phenotypes as compared to single morphants, but still yielded a spectrum from mild to severe (Figs. 2A–H; Supplemental Fig. S1; Table S1). In the mild phenotype, early morphogenesis of the eye cup was overtly normal, but by 36 hpf the choroid fissure failed to close (lines in Fig. 2F), a condition called coloboma. This ventral ocular defect was more evident in embryos showing moderate and severe phenotypes. In these embryos the eye lost its spherical shape and was often completely open on the ventral side (Figs. 2G, H). In addition, morphant eyes often appeared smaller with increased pyknotic cells as compared to controls (Figs. 2E–H). With regard to the variability in phenotypes, the efficiency of normal transcript splicing was disrupted in a manner that correlated with mild versus severe classes. However, we also found that the proportion of mild versus severe phenotypes varied with the genetic background of the injected embryos. Together this suggests that Lmx1b function is both dosage-sensitive and can be modified by genetic background.

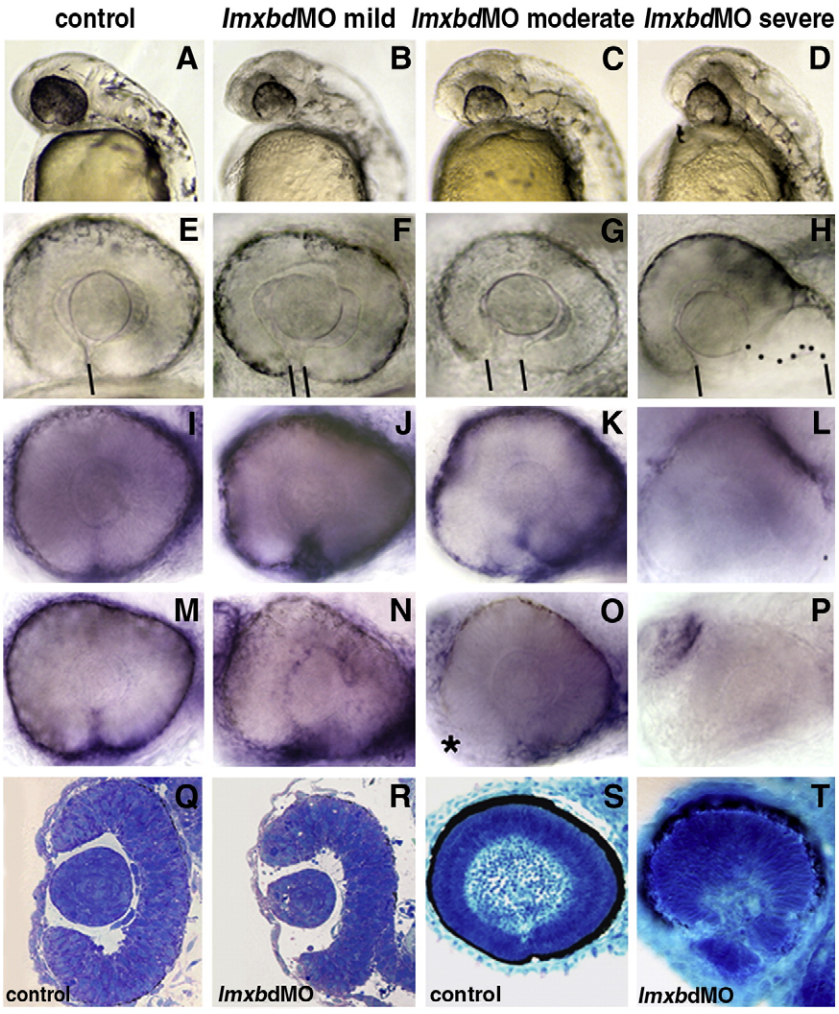

Fig. 2. Lmx1b knock-down disrupts ocular morphogenesis to variable degrees. Lateral view of 24 hpf heads (A, D) and higher magnification of 36 hpf PTU-treated eyes (E, H) with anterior to the left. (A–P) Control embryos and embryos with different degree of severity of the Lmx1b morpholino phenotypes as indicated on the top of each column. (H) Dots highlight the shape of the ventral retina. (E–H) Bars indicate the choroid fissure, which fails to close in the MO-injected embryos. Transcripts for *foxc1a* (I–L) and *eya2* (M–P) in control MO and differently affected *lmx1b*dMO morphant embryos as revealed by whole mount in situ hybridization at 36 hpf. Reduction of periocular cells was observed in anterior-ventral regions of moderate *lmx1b*dMO embryos (asterisk in panel O) and completely absent in severe morphants (L, P). Toluidine blue-stained transverse (Q, R) and sagittal (S, T) sections from control (Q, S) and moderate *lmx1b*dMO phenotypes (R, T) at 24 hpf and 62 hpf, respectively.

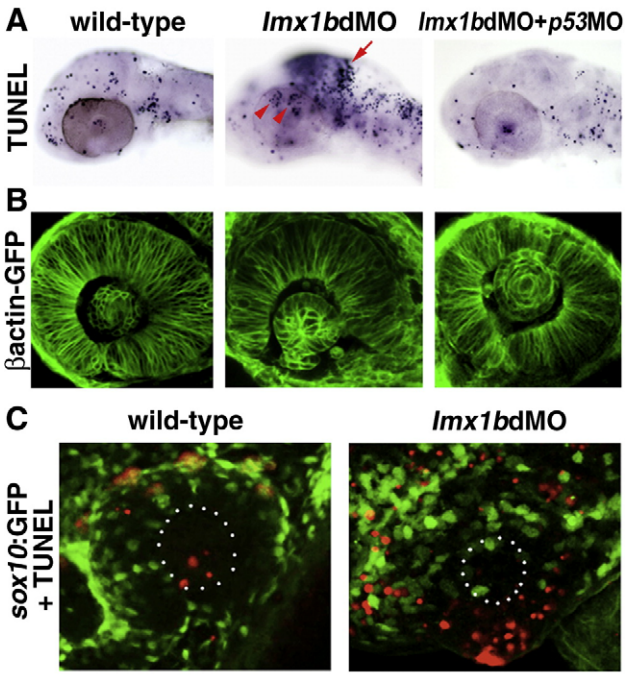

Fig. 3. Lmx1b loss of function induces apoptosis of Lmx1b expressing cells. (A) TUNEL staining of apoptotic cells (dark blue, top row) in *lmx1b*dMO morphants and *lmx1b*dMO morphants co-injected with p53MO and analyzed at 36 hpf. Red arrow indicates increased apoptosis in the midbrain–hindbrain boundary. Red arrowheads show increased periocular cell death in *lmx1b*dMO eyes. (B) Eye morphology in embryos corresponding to the above panel as visualized in the betaactinGFP transgenic line. (C) TUNEL staining (red) in *sox10*:GFP-positive neural crest cells (green) in wild-type and *lmx1b*dMO morphant eyes. White dots in B outline the lens.

Histological analysis of 24 hpf *lmx1b*dMO morphant eyes exhibiting a moderate phenotype showed a thinned retinal neuroepithelium and loosely organized periocular mesenchyme, with increased numbers of pyknotic nuclei, particularly in the ventral region (Figs. 2Q, R). At 62 hpf, when retinal lamination was apparent in control eyes, laminar differentiation was delayed and ventral ocular tissue often appeared disorganized in *lmx1b*dMO morphants (Figs. 2S, T). In these embryos, the retinal pigment epithelium often appeared reduced and disorganized in the ventral retina (Fig. 2T).

Periocular mesenchyme is compromised in lmx1bdMO morphants

Because *lmx1b* genes are expressed in periocular mesenchyme cells, we next assessed for changes in expression of markers of this population of cells that may accompany the eye defects in the *lmx1b*dMO-injected embryos. In mild and moderate *lmx1bd*MO phenotypes, we observed that *foxc1a* and *eya2* expressing periocular mesenchyme cells were able to migrate to the eye despite the loss of Lmx1b activity. In some cases, we detected an accumulation of periocular mesenchyme at the choroid fissure (Figs. 2J, N) and in more affected embryos, periocular cell migration towards the nasal-ventral region of the eye was altered (asterisk in Fig. 2O; Fig. 7). This suggests a defect in migration of periocular mesenchymal cells to defined locations of the eye. In severely affected *lmx1b*dMO morphants, periocular expression of *foxc1a* and *eya2* was almost absent, suggesting either a loss of marker gene expression or failure of periocular mesenchyme cells to arrive to the eye (Figs. 2L, P). Consistent with disruptions to periocular mesenchyme, vascular patterning was affected in the eyes of *lmx1b*dMO morphants at later stages (Supplemental Fig. S2). This data suggests that the most severe ocular phenotypes could be due to a loss of periocular mesenchyme, but that the mild and moderate ocular phenotypes cannot simply be due to the absence of these cells.

Lmx1b regulates survival of periocular mesenchyme cells

Knockout of *lmx1b* in mice leads to altered regulation of differentiation markers in anterior segment cells originating from periocular mesenchyme (Pressman et al., 2000). Histological inspection of *lmx1b* morphants suggested that in zebrafish loss of *lmx1b* in zebrafish results in apoptosis as well as differentiation defects in periocular mesenchyme. To assess apoptosis in *lmx1b*dMO morphants, we performed TUNEL analysis which revealed significantly elevated cell death in regions where *lmx1b* genes are normally expressed, most notably at the MHB and in cells around the eye (Fig. 3A, middle). Depletion of p53, a protein required for apoptosis under many conditions, blocked the regionally-localized cell death observed in *lmx1b*dMO embryos (Fig. 3A, right). Furthermore, overall eye size defects and ventral ocular dysgenesis were abrogated when apoptosis was inhibited, as observed using transgenic embryos in which individual cells were highlighted by expression of beta-actin-GFP (Tg(*Bactin*:HRAS-EGFP)^{vu119} ; Cooper et al., 2005) (Fig. 3B).

When apoptotic cells were labeled in transgenic morphant embryos expressing GFP in neural crest cells (Tg(−7.2*sox10*:EGFP)^{zf77}; Hoffman et al., 2007) there was minimal co-localization at 36 hpf (Fig. 3C). However, neural crest cells were depleted from the ventral eye and

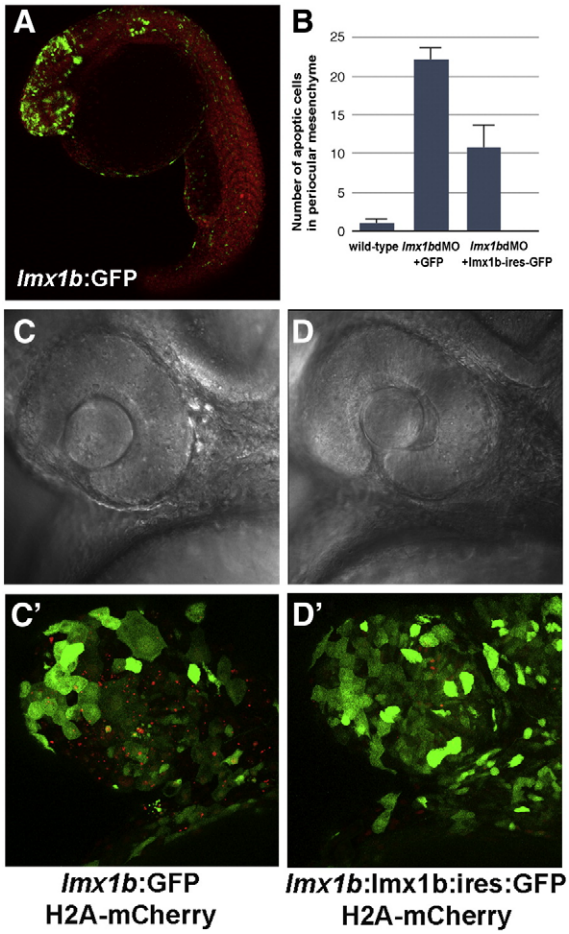

Fig. 4. Apoptosis in lmx1bdMO morphants is rescued by expression of lmx1b.1 cDNA. (A) Expression of GFP driven by the −5 kb *lmx1b.1* promoter. (B) Quantitation of the number of pyknotic cells present in ocular regions from wild-type, *lmx1b*dMO morphants expressing GFP, and *lmx1b*dMO embryos expressing lmx1b.1:ires:GFP. For each condition, $n = 10$ independent eyes were scored. Error bars represent Standard Error of the Mean. (C) Bright field image of *lmx1b*dMO morphants expressing GFP or (D) *lmx1b*dMO morphants expressing *lmx1b.1*:ires:GFP. (C′) Fluorescent image of panel C showing *lmx1b*:GFP-positive periocular cells (green) and pyknotic cells red). (D′) Fluorescent image of panel D showing *lmx1b*:lmx1b.1:ires:GFP-positive periocular cells (green) and pyknotic periocular cells (red).

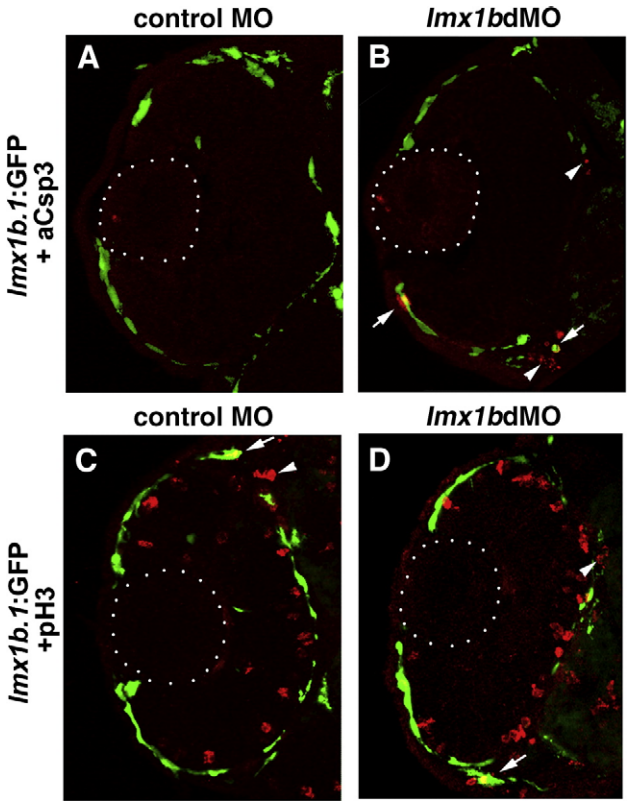

Fig. 5. Apoptosis and proliferation in *lmx1b.1*:GFP-positive cells following loss of Lmx1b function. (A) Immunoreactivity for activated Caspase-3 (red) and fluorescence for *lmx1b.1*:GFP^{mw11} (green) in control MO or (B) *lmx1b*dMO ocular cryosections at 36 hpf. Arrows indicate cells positive for both activated Caspase-3 and *lmx1b.1*:GFP, while arrows indicate GFP-negative apoptotic cells. (C) Immunoreactivity for phosphoHistone (red) and fluorescence for *lmx1b.1*:GFP^{mw11} (green) in control MO or (D) *lmx1b*dMO ocular cryosections at 36 hpf. Arrows indicate cells positive for both activated phosphoHistone-3 and *lmx1b.1*:GFP, while arrows indicate GFP-negative mitotic periocular cells. Dotted lines indicate position of the lens. Images shown are from representative sections ($n=24$ total embryos for each condition from 2 experiments).

apoptotic cells were numerous in this region (Fig. 3C). This suggests that the GFP in the neural crest cells was degraded by the time that the cells became TUNEL-positive. Additionally, some apoptotic periocular cells may be mesoderm-derived and therefore did not express the transgene.

To more directly evaluate whether cell death in embryos injected with *lmx1b* morpholinos was due to specific loss of Lmx1b function and not to off-target effects, we first attempted to rescue apoptosis by co-injecting *lmx1b* mRNA with morpholinos. However, global expression of either *lmx1b.1* or *lmx1b.2* mRNA resulted in severe gastrulation defects. To more faithfully express *lmx1b* cDNAs in endogenous locations, we isolated 5 kilobases (kb) of sequence directly upstream of the *lmx1b.1* gene and utilized this sequence to drive GFP expression (tol2:−5*lmx1b*:GFP). This tol2-based construct resulted in GFP accumulation in regions similar to that of endogenous *lmx1b.1* mRNA expression (Fig. 4A). We also generated a tol2-based expression construct where the 5 kb *lmx1b.1* promoter sequence was placed in front of the *lmx1b.1* cDNA, followed by an internal ribosome entry site (ires) proximal to GFP (tol2:−5*lmx1b.1*:lmx1b:ires:GFP). This construct was co-injected with *lmx1b* morpholinos into transgenic, H2A-mCherry embryos (Tg(*h2afx*:H2A-mCherry)^{mw3}). Expression of the nuclear-localized mCherry fluorescent protein revealed condensed chromatin of pyknotic cells when imaged at sub-threshold gain.

Expression of *lmx1b.1* cDNA under the control of its endogenous −5 kb promoter rescued much of the cell death associated with injection of the *lmx1b*dMO (Figs. 4B, D). Expression of GFP alone did not prevent morpholino-induced cell death (Figs. 4B, C). Together these data suggest that loss of Lmx1b activity results in apoptosis of periocular mesenchymal cells, which normally regulate ocular patterning and morphogenesis.

To better evaluate the consequences of Lmx1b depletion on *lmx1b*-positive cells, we established four independent transgenic lines using the tol2:−5*lmx1b*:GFP construct (Tg(−5 kb*lmx1b.1*:GFP)$^{mw10-13}$). Each line showed a high degree of specific overlap between GFP expression and endogenous *lmx1b.1* expression. Using cryosections from Tg(−5 kb*lmx1b.1*:GFP)^{mw11} embryos, we further assessed the pattern of cell death and proliferation for *lmx1b.1*:GFP-positive cells following injection of control or *lmx1b*dMO oligonucleotides. Immunoreactivity of activated Caspase-3, a marker of apoptotic cells, confirmed TUNEL analyses and showed that both *lmx1b.1*:GFP-positive and *lmx1b.1*:GFP-negative periocular cells displayed elevated apoptosis following depletion of Lmx1b activity (Figs. 5A, B). For phosphoHistone-3 immunoreactivity, which marks cells in the late G2/M-phase of the cell cycle, we did not find differences between

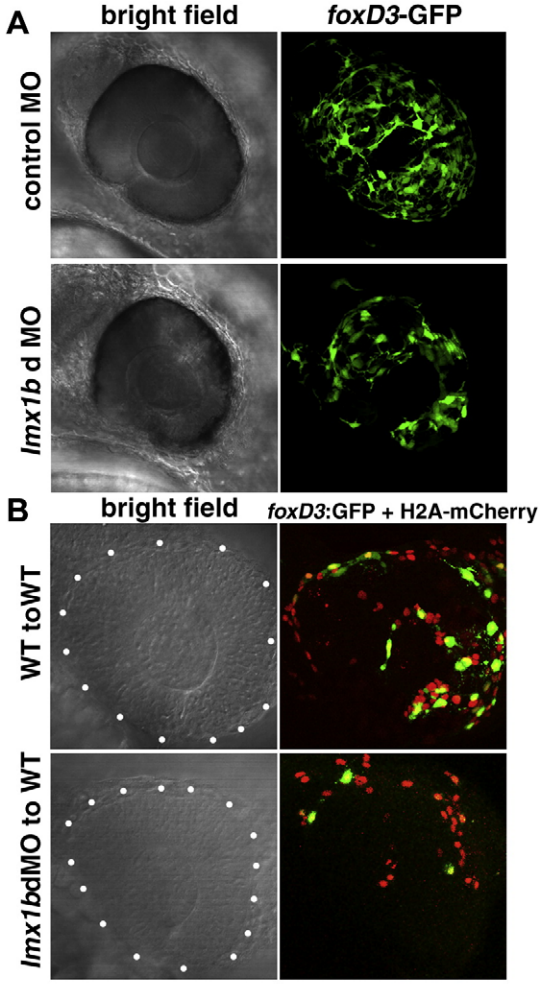

C

Donor cell origin	Ave. # *foxD3*:GFP+	Ave. # H2A-mCherry+	Percent
wild-type	19.8 ± 3.1	35.8 ± 5.3	55%
*lmx1b*dMO	2.8 ± 1.0	15.3 ± 3.2	18%

Fig. 6. Lmx1b functions cell-autonomously in development of periocular mesenchymal cells. (A) Bright field and fluorescent images of control MO and *lmx1b*dMO eyes showing *foxD3*:GFP-positive periocular mesenchymal cells. (B) Ocular region (outlined by white dots) of 30 hpf mosaic embryos showing wild-type or *lmx1b*dMO morphant donors. All donor cell nuclei are positive for H2A:mCherry (red), while a subset of periocular cells are positive for *foxD3*:GFP (green). (C) Average number ± Standard Error of the Mean for total H2A:mCherry and *foxD3*:GFP-positive donor periocular cells from mosaic embryos. Percent of total periocular cells that were foxD3-positive is shown in the right-most column. For each condition, donor cells from $n=12$ independent eyes were scored.

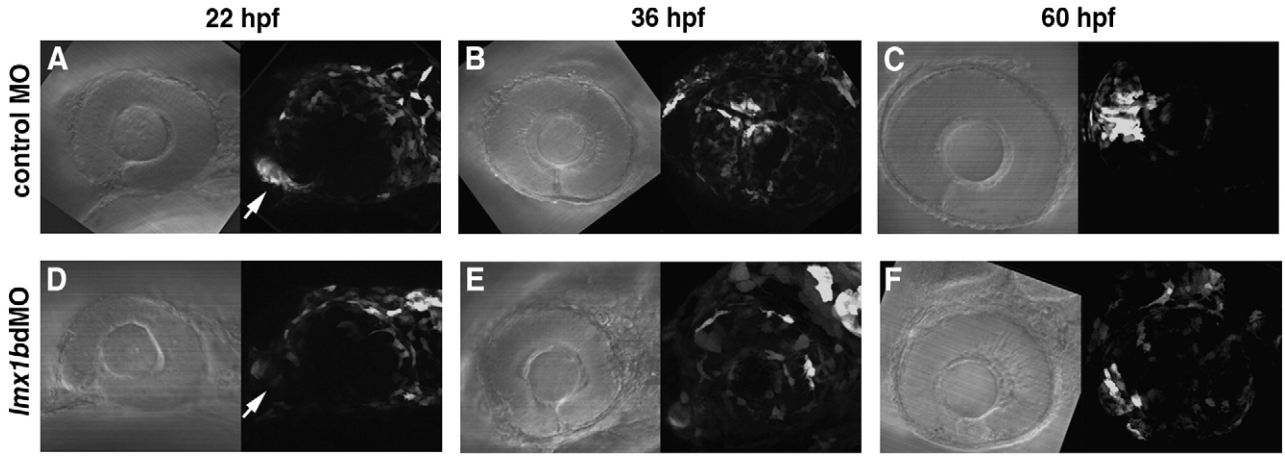

Fig. 7. Migration of *lmx1b.1*:GFP-positive cells is altered following knock-down of Lmx1b. Bright field and fluorescence images of (panels A–C) control MO and (panels D–F) *lmx1b*dMO embryos from the Tg(−5 kb *lmx1b.1*:GFP)^{mw11} line. For each image developmental time is indicated at the top, anterior is to the left, and dorsal is up. Arrows indicate the location of the optic stalk region. (D) Note the significant reduction of GFP fluorescence in Lmx1b-deficient cells associated with the optic stalk. Each fluorescent image is a compressed *z*-stack, which includes the entire globe of the eye and optic stalk region. Images shown are from representative embryos ($n = 12$ total embryos tracked over time from 2 experiments).

control and *lmx1b*dMO eyes (Figs. 5C, D). However, proliferation of periocular mesenchymal cells in either control or *lmx1b*dMO eyes was rare.

Loss of lmx1b cell-autonomously compromises periocular cells

Periocular cell death and differentiation defects in *lmx1b*dMO morphants may still be due to secondary defects caused by loss of Lmx1b function in the ventral diencephalon. To address this possibility, we generated genetic mosaic embryos in which small groups of cells with compromised Lmx1b activity were located in otherwise wild-type embryos. Donor embryos were derived by mating Tg(*foxd3*:GFP)^{zf15} and Tg(*h2afx*:H2A-mCherry)^{mw3} transgenic fish in order to label all donor cells with the H2A-mCherry transgene and periocular neural crest donor cells with the *foxD3*:GFP transgene (Fig. 6A). Hosts embryos were always derived from non-transgenic, wild-type parents. Comparisons were made between *lmx1b*dMO-injected and non-injected donor cells to address the autonomy of Lmx1b activity on periocular mesenchymal cell apoptosis and migration defects. Following the transplantation of blastulae cells into regions fated for neural crest, mosaic embryos were fixed at 30 hpf. To ensure that neural crest targeting was achieved, embryos were screened for at least one mCherry-positive nucleus in the ocular mesenchyme and none in the ventral forebrain. Wild-type and *lmx1b*dMO donor mosaic embryos were scored for the number of H2A-mCherry and *foxD3*:GFP-positive periocular cells. Host embryos with donor cells deficient for Lmx1b function showed significant reduction in both the total number of donor cells in the periocular region and *foxD3*:GFP-positive cells (Figs. 6B, C). Like embryos in which *lmx1b* genes were knocked-down globally, *lmx1b*-deficient periocular mesenchymal cells tended to accumulate dorsally and posteriorly within wild-type host eyes (Fig. 6B, lower right). In addition to periocular mesenchyme, mosaic embryos from either condition showed equivalent contributions to non-ocular structures, indicating that wild-type and *lmx1b*dMO donor cells transplanted with similar efficiencies. Furthermore, mismatch control morpholino donor cells showed similar distribution and number of periocular mesenchymal cells as compared to wild-type donor cells.

These results indicate that the *lmx1b* genes function cell-autonomously in periocular cells to regulate their survival and potentially normal migration. Evidence supporting a role for periocular mesenchyme in eye patterning has been previously reported (Fuhrmann et al. 2000; Matt et al., 2005; Lupo et al., 2005; Molotkov et al., 2006; Matt et al. 2008). For these reasons, we explored the consequences of abrogation of Lmx1b function first on periocular cell migration and then on retinal morphogenesis and patterning.

Depletion of Lmx1b alters periocular cell migration and positioning within the eye

To directly evaluate lmx1b-positive periocular cell migration we injected Tg(−5 kb *lmx1b.1*:GFP)^{mw10} and Tg(−5 kb*lmx1b.1*:GFP)^{mw11} embryos with equal concentrations of either mismatch control morpholinos or the *lmx1b*dMO cocktail. Between 20 and 60 hpf, the location of GFP-positive cells was assessed in control or *lmx1b*dMO embryos. We found that *lmx1b.1*:GFP expression was significantly

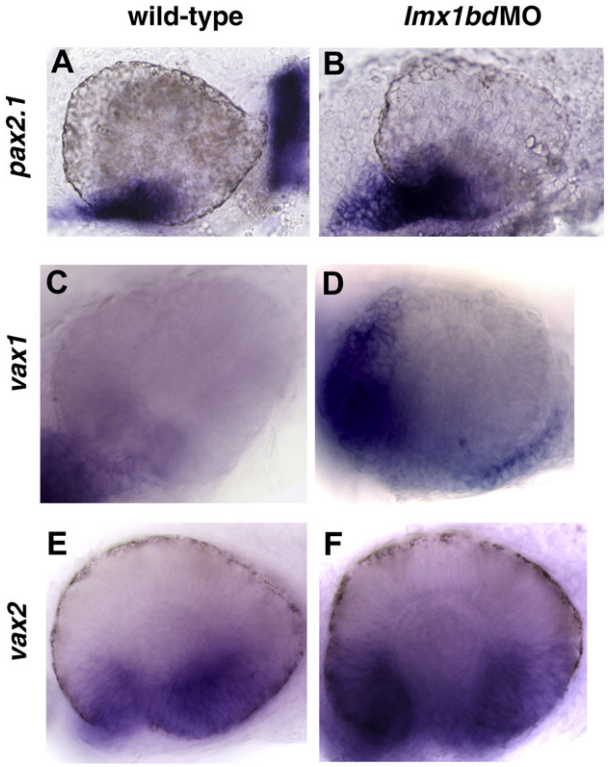

Fig. 8. Lmx1b loss of function promotes the expansion of ventral ocular markers. Transcripts for *pax2.1* (A, B), *vax1* (C, D), *vax2* (E, F) detected by whole mount in situ hybridization in uninjected control and *lmx1b*dMO embryos at 24 hpf.

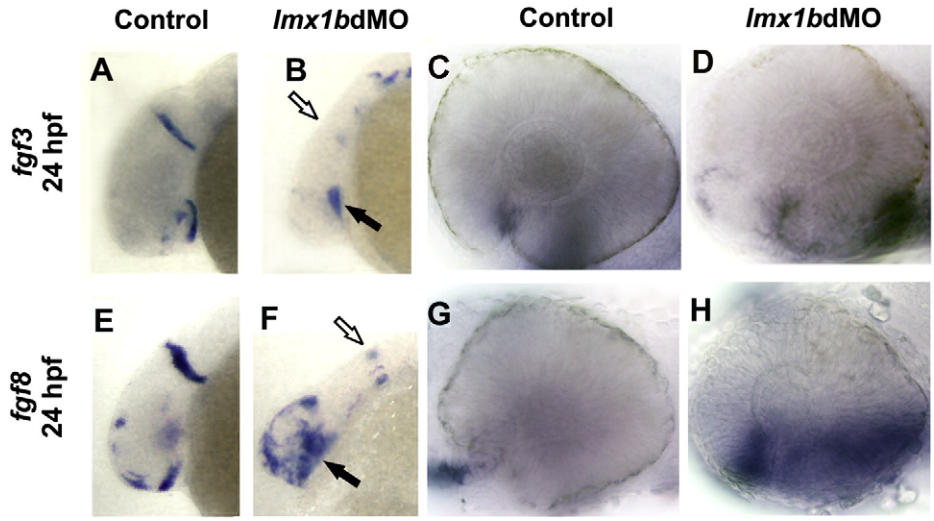

Fig. 9. Fgf signaling is activated in lmx1b morphant ocular regions. Whole mount in situ hybridization for *fgf3* (A–D) and *fgf8* (E–H) in control and *lmx1b*dMO embryos showing head (A, B, E, F) and higher magnification of the eyes (C, D, G, H). Note the expansion of *fgf3* and *fgf8* in optic stalk and ventral retinal tissues of *lmx1b*dMO embryos (solid arrows in panels B, F). In contrast, midbrain–hindbrain expression was decreased in *lmx1b*dMO morphant embryos (open arrows in panels B, F).

reduced within the optic stalk region throughout the period that this transgene was expressed there (21–30 hpf) (Figs. 7A, D arrows; Supplemental Fig. S3). When periocular cells arrived to the eye, the number of GFP-positive cells was equivalent in control and *lmx1b*dMO embryos (Figs. 7A, D). By 36 hpf, the number of *lmx1b.1*:GFP-positive cells were reduced and their location was altered. Specifically, in control embryos GFP-positive cells began to accumulate in a more anterior/nasal region, but GFP-positive cells tended to remain in a more posterior/temporal location in *lmx1b*dMO eyes (Figs. 7B, E). These differences were maintained throughout the efficacy of morpholino knock-down (Figs. 7C, F). This experiment, along with the marker studies described above, suggests that loss of Lmx1b results in both elevated apoptosis and migration defects for periocular mesenchymal cells.

Loss of Lmx1b affects expression of neural retinal genes involved in ventral ocular morphogenesis

The ventral ocular defects and coloboma phenotype observed in *lmx1b*dMO morphants are reminiscent of defects caused by alteration to *pax2*, *vax1* and *vax2* expressions in the optic stalk and ventral neural retina (Macdonald and Wilson, 1996; Take-uchi et al., 2003). Therefore we analyzed the expression pattern of these transcripts in *lmx1b*dMO morphants exhibiting mild to moderate eye morphogenesis phenotypes.

As compared to 24 hpf uninjected controls, we observed expansion of *pax2.1* expression in the optic stalk and nasal retina of *lmx1b*dMO morphants (Figs. 8A, B). At 24 hpf, *vax1* and *vax2* are normally expressed in the optic stalk and preoptic area (Figs. 8C, E) and *vax2* is additionally expressed in the ventral retina. As compared to control embryos at 24 hpf, *vax1* expression was expanded in the ventral region of the optic cup in *lmx1b*dMO morphants, including cells within the presumptive retinal pigmented epithelium (Figs. 8C, D). Expression of *vax2* was also enhanced in the optic stalk and ventral retina, and slightly expanded into more nasal and temporal regions of the ventral retina (Fig. 8F). Because *lmx1b* genes are not obviously expressed directly within the ventral retina, these results indicate that Lmx1b activity in non-retinal cells, most probably periocular mesenchymal cells or those associated with the optic stalk, are required for ventral retinal development.

Fgf signaling is altered in lmx1b morphants

Fgfs are implicated in several aspects of ocular development, including optic cup patterning, retinogenesis, and anterior segment morphogenesis. For instance, Fgf activity from the optic stalk contributes to *vax* regulation (Take-uchi et al., 2003) and when Fgf signaling is increased in the optic stalk and periocular regions by the *aussicht* mutation, defects in optic fissure closure, ocular patterning and differentiation are observed (Heisenberg et al.,

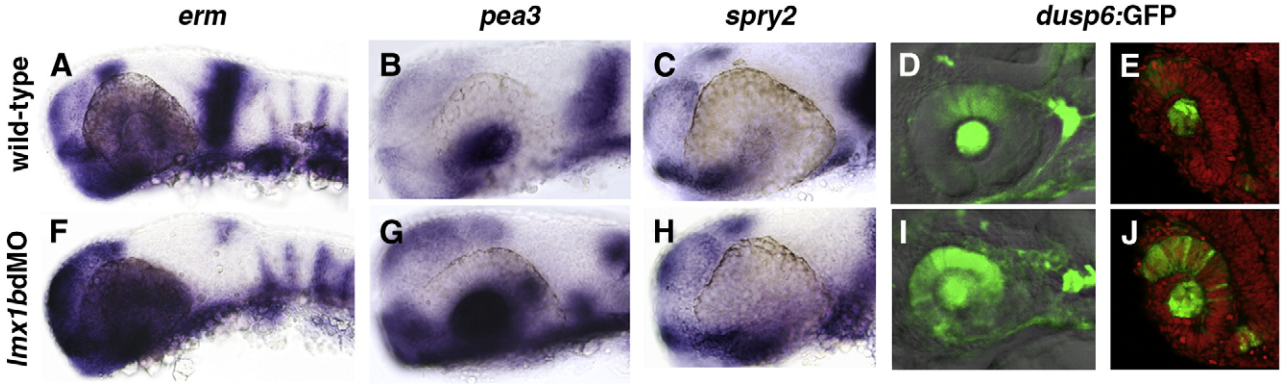

Fig. 10. Expression of Fgf-target genes is altered in *lmx1b* morphants. Whole mount in situ hybridization in 24 hpf embryos for *erm*, *pea3*, and *spry2* (A–C, F–H) and fluorescence in Tg (*dusp6*:dEGFP) (D, E, I, J). For each Fgf-target gene, note the expansion in periocular and ocular regions and reduction in the MHB. For *dusp6*:GFP, sections confirmed up-regulation of GFP in the dorsal neural retina, lens, and optic stalk regions (E, J). Sections were counter-stained with propidium iodide to highlight nuclei (red).

1999). To determine if ocular dysgenesis in *lmx1b* morphants involves altered Fgf signaling, we analyzed *fgf3* and *fgf8a* expression patterns in *lmx1b* morphants. At 18 s, *fgf3* expression in *lmx1b*dMO morphants appeared normal (data not shown). By 24 hpf, *lmx1b*dMO morphants revealed a slight alteration of *fgf3* expression in the rostral CNS and complete down-regulation in the MHB (Figs. 9A–D and O'Hara et al., 2005). Morphants displayed a more dramatic change in the pattern of *fgf8a*. At 18 s, *fgf8a* expression in the optic stalk region was moderately up-regulated in *lmx1b*dMO morphants (data not shown) and by 24 hpf, significantly expanded within the optic stalk, ventral retina and telencephalon (Figs. 9F–H).

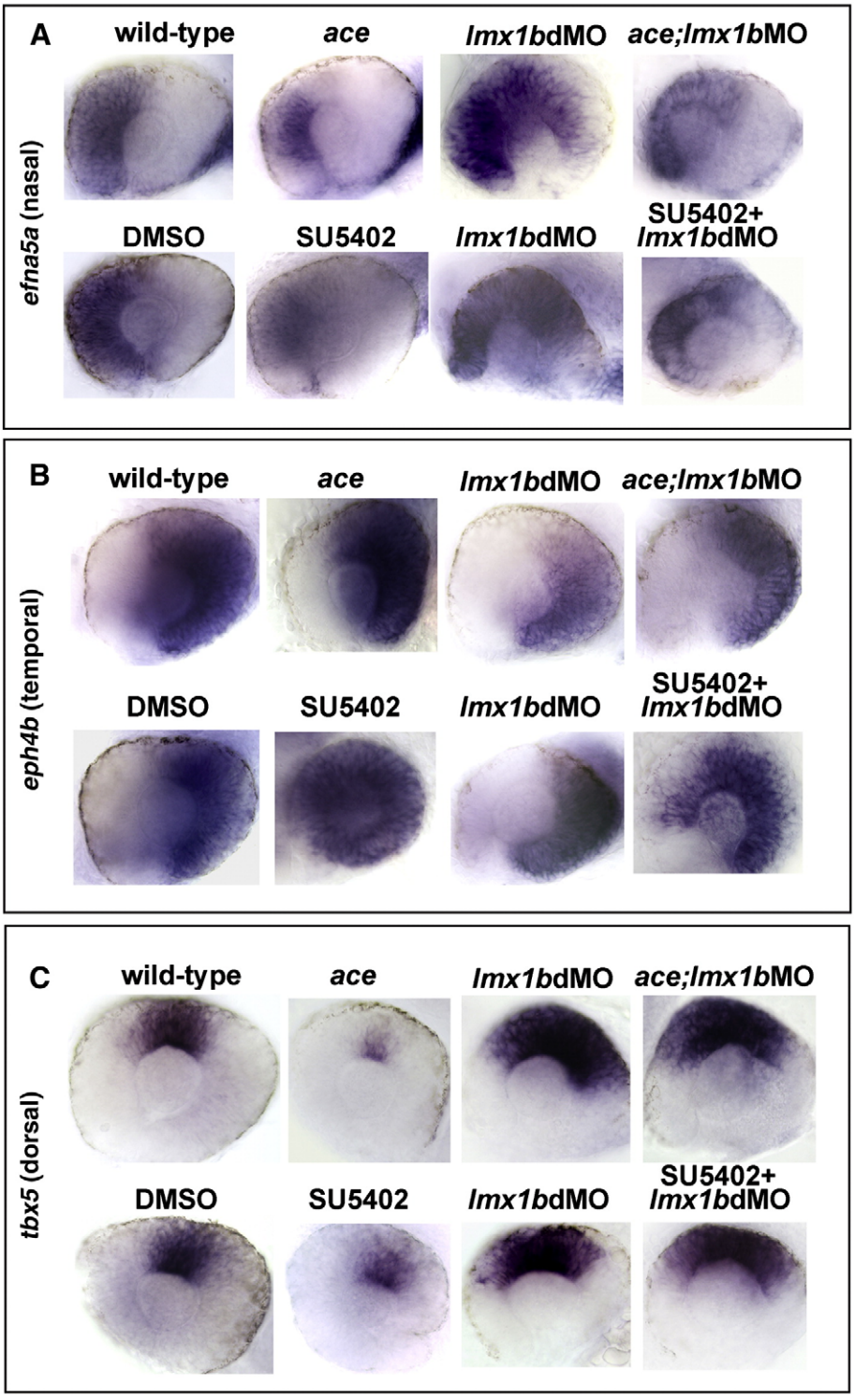

Fig. 11. Lmx1b is required for patterning the retina in a manner partially independent from Fgf signaling. Expression of nasal, temporal, and dorsal ocular markers with reduced Fgf signaling and Lmx1b function. Lateral view of 24 hpf eyes from whole mount in situ hybridization of (panel A) *efna5a* (nasal), (panel B) *eph4b* (temporal), and (panel C) *tbx5* (dorsal). Note the reduction of *efna5a* and *tbx5* markers in *fgf8a*/*ace* mutants or SU5402-treated embryos and expansion of these markers in *lmx1b* morphants. Partially rescued and intermediate phenotypes were observed when Fgf signaling was reduced in *lmx1b* morphants. With *eph4b*, expansion was noted in *fgf8a*/*ace* mutants or SU5402-treated embryos, while the opposite was found in *lmx1b* morphants. Again, intermediate phenotypes were observed when Fgf signaling was reduced in *lmx1b* morphants.

In reciprocal experiments, we performed expression analysis of *lmx1b* genes in *fgf3*, *fgf8a*, and *fgf3+fgf8a* morphants. At 24 hpf, forebrain and ocular expression of *lmx1b.1* and *lmx1b.2* was not significantly affected in the *fgf3*, *fgf8a* or *fgf3+fgf8a* morphants (Supplemental Fig. S4). However, subtle changes were observed within the MHB, perhaps owing to the essential role of Fgf3 and Fgf8a on the formation of this structure.

To address whether Fgf-mediated gene transcription was affected by compromising Lmx1b function, we analyzed various target genes of Fgf signaling in ocular regions including *erm*, *pea3*, *spry2*, and *dusp6*:GFP (Roehl and Nusslein-Volhard, 2001; Furthauer et al., 2002; Tsang et al., 2002; Raible and Brand, 2001; Molina et al., 2007). Upon knock-down of both *lmx1b* genes, all Fgf-regulated genes assessed were significantly up-regulated in the forebrain and eye tissues, but down-regulated in the MHB region (Fig. 10). Cryosections of *dusp6*:GFP, as well as adjusted-focus inspection of whole mount stained embryos, indicated the Fgf-target genes were up-regulated in the neural retina, optic stalk regions, and lens, but not in periocular cells. Together, these results suggest that Lmx1b negatively regulates ocular *fgf3* and *fgf8a* expression and activity.

Enhanced Fgf signaling contributes to, but is not fully responsible for, the retinal patterning defects upon depletion of Lmx1b

Fgf signals, including Fgf8, determine nasal-temporal patterning of the retina by promoting nasal and repressing temporal identity (Picker and Brand, 2005). Given that *lmx1b*dMO morphants showed an up-regulation of Fgf signaling in the eye, we assessed whether loss of Lmx1b function affected nasal-temporal patterning of the retina. Indeed, the nasal marker *efna5a* and dorsal marker *tbx5* were both expanded in *lmx1b*dMO morphants (Figs. 11A, C). Conversely, the temporal marker *epha4b* was reduced following loss of *lmx1b* genes (Fig. 11B).

In order to evaluate the relationships between Lmx1b and Fgf signaling, we analyzed the consequences of loss of *lmx1b* function in the *fgf8a* mutant *acerebellar* (*ace*). As already reported, the expression of *tbx5* and *efna5a* were reduced and *epha4b* expanded in *fgf8a*/*ace* mutants (Fig. 11; Picker and Brand, 2005). Loss of Fgf8a activity in *lmx1bd*MO morphants led to phenotypes intermediate between control and Lmx1b-deficient conditions. This suggests that some of the consequences of loss of Lmx1b function are dependent upon Fgf8 signaling.

To more severely abrogate Fgf signaling in *lmx1b* morphants, Fgf receptor activity was inhibited with SU5402 starting at the 6 somite stage. In agreement with a previous study (Picker and Brand, 2005), SU5402-treated embryos showed more severe naso-temporal patterning defects (Figs. 11A–C). Although SU5402 treatment of *lmx1b*dMO morphants partially restored nasal and temporal expression patterns, *tbx5* remained expanded in the dorsal retina and embryos still showed ventral ocular dysgenesis (Fig. 11B). Together, these experiments suggest that increased Fgf activity in *lmx1b*dMO embryos is partially, but not fully, responsible for the ocular defects caused by loss of Lmx1b function.

Discussion

In this study, we describe the expression and consequences of loss of function of *lmx1b.1* and *lmx1b.2* during zebrafish ocular morphogenesis. As previously reported for other vertebrates, *lmx1b.1* and *lmx1b.2* are expressed in periocular mesenchymal cells. Here we show that together they are required cell-autonomously for migration and survival of these cells. Lmx1b has a cell-non-autonomous requirement for ventral eye morphogenesis, closure of the choroid fissure and retinal pattering. Finally, levels of Fgf signaling are dependent upon Lmx1b activity and enhanced Fgf activity is partially responsible for retinal patterning phenotypes observed in Lmx1b morphants.

Lmx1b in the periocular mesenchyme is crucial for eye morphogenesis

Early in development, the emerging eye is surrounded by periocular mesenchyme that contributes to specialized non-neural structures of the eye after morphogenesis is complete. Emerging evidence suggests that reciprocal interactions between the periocular mesenchyme and the retina are required for the correct morphogenesis of the eye. The retina plays a critical role in directing the migration of the periocular mesenchyme and once these cells are in place, signals such as retinoic acid (RA) act in a paracrine manner to regulate expression of the periocular mesenchyme genes such as *pitx2*, *eya2* and *foxc1* (Matt et al., 2005; Molotkov et al., 2006; Langenberg et al., 2008; Matt et al., 2008). Here we suggest that reciprocally, the periocular mesenchyme is necessary for the proper morphogenesis of the ventral eye. In addition, it is possible that lmx1b-positive cells of the ventral forebrain also influence ocular patterning. However, unlike lmx1b-positive periocular cells, the ventral forebrain cells are not overtly affected by loss of Lmx1b function. Indeed, the primary cause for ocular dysgenesis and coloboma upon loss of Lmx1b function appears to be apoptosis of periocular mesenchyme associated with the optic stalk and globe of the eye, as the visible ocular phenotypes following knock-down of *lmx1b* are rescued by blocking apoptosis. A similar requirement for signaling from the periocular mesenchyme has been proposed in mice, as impairing RA signaling from neural crest cells is sufficient to alter eye morphogenesis (Molotkov et al. 2006; Matt et al., 2008). Disrupting RA signaling appears to affect morphogenesis but not axial patterning, whereas upon Lmx1b knock-down, we observed significant defects in both dorso-ventral and naso-temporal patterning. This suggests that other signaling pathways, such as Fgf, are likely involved in the reciprocal cross talk between periocular mesenchyme and retina. Our studies, combined with those of others, point to the requirement for complex interactions between periocular mesenchyme and retina for patterning and morphogenesis. Notably, disrupting this cross talk gives rise to coloboma, a common yet poorly understood ocular defect.

Evolutionarily conserved and novel phenotypes with loss of Lmx1b function in zebrafish

Lmx1b functions in various embryonic structures, and loss-of-function phenotypes have been described in humans, mice, and zebrafish (Dreyer et al., 1998; Vollrath et al., 1998; Chen et al., 1998; O'Hara et al., 2005). In this paper we report a new role for Lmx1b in ocular morphogenesis. In humans, heterozygous loss-of-function mutations result in Nail-Patella Syndrome. These patients are prone to develop glaucoma, but do not show visible ocular dysmorphogenesis (Lichter et al., 1997). This phenotype is potentially the result of subtle developmental defects that sensitize individuals to glaucoma. It is difficult to directly compare zebrafish with the human phenotypes given that homozygous *LMX1B* mutations have not been observed and likely cause early embryonic lethality. In contrast to humans, heterozygous loss-of-function mutations in mouse *lmx1b* do not result in obvious phenotypes, although extensive analysis on multiple genetic backgrounds has not been described. Homozygous null mutations in mice do result in ocular defects but they are considerably milder than those seen in zebrafish morphants (Pressman et al., 2000). In the mouse eye, *lmx1b* −/− mutations primarily affect differentiation, and not survival or migration of periocular mesenchyme. Furthermore the dorso-ventral differences in the severity of the fish eye phenotypes are not evident in mouse mutants. However, the normal dorso-ventral anatomical differences in the zebrafish anterior segment are much more striking than in mammals (Soules and Link, 2005). One similarity is that in both zebrafish morphants and mouse mutants, the overall eye size is often small, suggesting a conserved non-cell-autonomous role for Lmx1b in ocular growth. Furthermore, for all vertebrates analyzed Lmx1b is required for cell survival within

MHB tissues. Nonetheless, while Lmx1b function is strongly conserved in its requirement for cell survival in the isthmo-cerebellar region, Lmx1b has a more critical role in eye development for fish than mouse.

Although different thresholds for Lmx1b are required for humans and mice, *lmx1b* phenotypes have relevance to anterior segment development and glaucoma in both species. Similar to other species, we find zebrafish *lmx1b* is expressed in periocular mesenchyme cells that contribute to anterior segment structures. In addition, we observed a range of eye phenotypes of differing severity following loss of Lmx1b function, the milder of which may be more analogous to the human phenotypes and have relevance to glaucoma. In these zebrafish morphant phenotypes, the expression patterns of *foxc1* (Fig. 2) and *pitx2* (data not shown), key regulators of anterior eye segment development and risk genes for glaucoma, were disturbed. We observed accumulations of both *lmx1b* and *foxc1*-expressing cells associated with defects in their migration towards the nasal-ventral region of the eye and into the eye cup. Accumulations of *foxc1*- and *eya2*-expressing cells in the ventral part of the eye are unlikely due to increased apoptosis and are more likely a consequence of abnormal migratory behavior or defects in differentiation. Alterations in the periocular location of *lmx1b.1*:GFP-positive cells at multiple time-points more directly demonstrate defects in cell migration. Given the limitations of long-term gene knock-down using morpholinos, we did not determine the late consequences of Lmx1b depletion on periocular mesenchyme differentiation. However, it is likely that prolonged *lmx1b* knock-down would lead to anterior segment dysgenesis. Thus future studies are needed to determine if permanent reduction of Lmx1b function leads to anterior segment dysgenesis and other glaucoma-associated phenotypes in zebrafish.

Lmx1b regulates signaling networks in multiple tissues

Lmx1b is essential for transcriptional network regulation during development in multiple organ systems. For example, Lmx1b specifies dorsal-ventral identity in the limb bud mesenchyme (Chen and Johnson, 2002) and as part of its organizing function in this tissue, Lmx1b non-autonomously regulates motorneuron trajectory (Kania et al., 2000). Lmx1b is also essential for the appropriate regulation of organizing activity in the MHB (O'Hara et al., 2005; Matsunaga et al., 2002; Guo et al., 2007; this study). In this region, Lmx1b maintains other factors, such as *pax2*, that promote *fgf8* transcription (O'Hara et al., 2005). In agreement with that study, we found diminished *fgf8* expression in the MHB of *lmx1b*dMO embryos. In contrast to the MHB, within the eyes loss of Lmx1b function resulted in up-regulation of Fgf signaling.

Fgf signaling promotes nasal and represses temporal retinal identity (Picker and Brand, 2005) and we observed similar results from Lmx1b loss-of-function experiments. In our experiments, Fgf and Lmx1b act antagonistically and reduction of both factors are closer to wild-type than phenotypes resulting from loss of either Fgf signaling or Lmx1b function alone. However, epistasis cannot solely explain the antagonistic relationship because blocking Fgf signaling only partially rescued the loss of Lmx1b function. Thus, loss of Lmx1b likely affects additional signaling pathways to cause ocular patterning and ventral eye morphogenesis defects. As Fgf functions together with RA and Hedgehog signaling during dorso-ventral patterning of the eye, these same signaling pathways are candidates for Lmx1b-mediated signaling (Lupo et al., 2005). Cumulatively, our studies combined with others demonstrate critical, but context-dependent functions for Lmx1b in coordinating signaling activities, including those mediated by Fgfs, to regulate cell proliferation, migration, fate-determination, and survival within multiple tissues.

Acknowledgments

This study was supported by grants F32EY16321 (CM), T32EY014537 (CM), R01EY16060 (BL), a Telethon Fellowship (GG), and grants from the MRC and Wellcome Trust (SW). We thank members of our labs for discussions and Pat Cliff, Melissa Reske, and Anitha Ponnuswami for technical help.

Appendix A. Supplementary data

Supplementary data associated with this article can be found, in the online version, at doi:10.1016/j.ydbio.2009.05.577.

References

Albertson, R., Yelick, P., 2005. Roles for fgf8 signaling in left–right patterning of the visceral organs and craniofacial skeleton. Dev. Biol. 283, 310–321.
Chen, H., Johnson, R.L., 2002. Interactions between dorsal–ventral patterning genes *lmx1b*, *engrailed-1* and *wnt-7a* in the vertebrate limb. Int. J. Dev. Biol. 46, 937–941.
Chen, H., Lun, Y., Ovchinnikov, D., Kokubo, H., Oberg, K.C., Pepicelli, C.V., Gan, L., Lee, B., Johnson, R.L., 1998. Limb and kidney defects in Lmx1b mutant mice suggest an involvement of LMX1B in human nail patella syndrome. Nat. Genet. 19, 51–55.
Cooper, M.S., Szeto, D.P., Sommers-Herivel, G., Topczewski, J., Solnica-Krezel, L., Kang, H.C., Johnson, I., Kimelman, D., 2005. Visualizing morphogenesis in transgenic zebrafish embryos using BODIPY TR methyl ester dye as a vital counterstain for GFP. Dev. Dyn. 232, 359–368.
Cvekl, A., Tamm, E.R., 2004. Anterior eye development and ocular mesenchyme: new insights from mouse models and human diseases. BioEssays 26, 374–386.
Dreyer, S.D., Zhou, G., Baldini, A., Winterpacht, A., Zabel, B., Cole, W., Johnson, R.L., Lee, B., 1998. Mutations in LMX1B cause abnormal skeletal patterning and renal dysplasia in nail patella syndrome. Nat. Genet. 19, 47–50.
Dunston, J.A., Reimschisel, T., Ding, Y.Q., Sweeney, E., Johnson, R.L., Chen, Z.F., McIntosh, I., 2005. A neurological phenotype in nail patella syndrome (NPS) patients illuminated by studies of murine Lmx1b expression. Eur. J. Hum. Genet. 13, 330–335.
Filippi, A., Durr, K., Ryu, S., Willaredt, M., Holzschuh, J., Driever, W., 2007. Expression and function of nr4a2, lmx1b, and pitx3 in zebrafish dopaminergic and noradrenergic neuronal development. BMC Dev. Biol. 7, 135.
Fuhrmann, S., Levine, E.M., Reh, T.A., 2000. Extraocular mesenchyme patterns the optic vesicle during early eye development in the embryonic chick. Development 127, 4599–4609.
Furthauer, M., Lin, W., Ang, S.L., Thisse, B., Thisse, C., 2002. Sef is a feedback-induced antagonist of Ras/MAPK-mediated FGF signalling. Nat. Cell Biol. 4, 170–174.
Gage, P.J., Suh, H., Camper, S.A., 1999. Dosage requirement of Pitx2 for development of multiple organs. Development 126, 4643–4651.
Gage, P.J., Rhoades, W., Prucka, S.K., Hjalt, T., 2005. Fate maps of neural crest and mesoderm in the mammalian eye. Invest. Ophthalmol. Vis. Sci. 46, 4200–4208.
Gilmour, D.T., Maischein, H.M., Nusslein-Volhard, C., 2002. Migration and function of a glial subtype in the vertebrate peripheral nervous system. Neuron 34, 577–588.
Gould, D.B., Smith, R.S., John, S.W., 2004. Anterior segment development relevant to glaucoma. Int. J. Dev. Biol. 48, 1015–1029.
Guo, C., Qiu, H.Y., Huang, Y., Chen, H., Yang, R.Q., Chen, S.D., Johnson, R.L., Chen, Z.F., Ding, Y.Q., 2007. Lmx1b is essential for Fgf8 and Wnt1 expression in the isthmic organizer during tectum and cerebellum development in mice. Development 134, 317–325.
Heisenberg, C.P., Brennan, C., Wilson, S.W., 1999. Zebrafish aussicht mutant embryos exhibit widespread overexpression of ace (fgf8) and coincident defects in CNS development. Development 126, 2129–2140.
Ho, R., Kane, D., 1990. Cell-autonomous action of zebrafish spt-1 mutation in specific mesodermal precursors. Nature 348, 728–730.
Hoffman, T.L., Javier, A.L., Campeau, S.A., Knight, R.D., Schilling, T.F., 2007. Tfap2 transcription factors in zebrafish neural crest development and ectodermal evolution. J. Exp. Zoolog. B Mol. Dev. Evol. 308, 679–691.
Johnston, M.C., Noden, D.M., Hazelton, R.D., Coulombre, J.L., Coulombre, A.J., 1979. Origins of avian ocular and periocular tissues. Exp. Eye Res. 29, 27–43.
Kania, A., Johnson, R.L., Jessell, T.M., 2000. Coordinate roles for LIM homeobox genes in directing the dorsoventral trajectory of motor axons in the vertebrate limb. Cell 102, 161–173.
Kawakami, K., 2005. Transposon tools and methods in zebrafish. Dev. Dyn. 234, 244–254.
Kidson, S.H., Kume, T., Deng, K., Winfrey, V., Hogan, B.L., 1999. The forkhead/winged-helix gene, *Mf1*, is necessary for the normal development of the cornea and formation of the anterior chamber in the mouse eye. Dev. Biol. 211, 306–322.
Kimmel, C.B., Ballard, W.W., Kimmel, S.R., Ullmann, B., Schilling, T.F., 1995. Stages of embryonic development of the zebrafish. Dev. Dyn. 203, 253–310.
Kwan, K.M., Fujimoto, E., Grabher, C., Mangum, B.D., Hardy, M.E., Campbell, D.S., Parant, J.M., Yost, H.J., Kanki, J.P., Chien, C.B., 2007. The Tol2kit: a multisite gateway-based construction kit for Tol2 transposon transgenesis constructs. Dev. Dyn. 236, 3088–3099.
Langenberg, T., Kahana, A., Wszalek, J.A., Halloran, M.C., 2008. The eye organizes neural crest cell migration. Dev. Dyn. 237, 1645–1652.
Lawson, N.D., Weinstein, B.M., 2002. In vivo imaging of embryonic vascular development using transgenic zebrafish. Dev. Biol. 248, 307–318.
Lichter, P.R., Richards, J.E., Downs, C.A., Stringham, H.M., Boehnke, M., Farley, F.A., 1997. Cosegregation of open-angle glaucoma and the nail-patella syndrome. Am. J. Ophthalmol. 124, 506–515.
Lupo, G., Liu, Y., Qiu, R., Chandraratna, R.A., Barsacchi, G., He, R.Q., Harris, W.A., 2005. Dorsoventral patterning of the *Xenopus* eye: a collaboration of Retinoid, Hedgehog and FGF receptor signaling. Development 132, 1737–1748.
Macdonald, R., Wilson, S.W., 1996. Pax proteins and eye development. Curr. Opin. Neurobiol. 6, 49–56.

Matsunaga, E., Katahira, T., Nakamura, H., 2002. Role of Lmx1b and Wnt1 in mesencephalon and metencephalon development. Development 129, 5269–5277.
Matt, N., Dupe, V., Garnier, J.M., Dennefeld, C., Chambon, P., Mark, M., Ghyselinck, N.B., 2005. Retinoic acid-dependent eye morphogenesis is orchestrated by neural crest cells. Development 132, 4789–4800.
Matt, N., Ghyselinck, N.B., Pellerin, I., Dupe, V., 2008. Impairing retinoic acid signalling in the neural crest cells is sufficient to alter entire eye morphogenesis. Dev. Biol. 320, 140–148.
Maves, L., Jackman, W., Kimmel, C.B., 2002. FGF3 and FGF8 mediate a rhombomere 4 signaling activity in the zebrafish hindbrain. Development 129, 3825–3837.
Mears, A.J., Jordan, T., Mirzayans, F., Dubois, S., Kume, T., Parlee, M., Ritch, R., Koop, B., Kuo, W.L., Collins, C., Marshall, J., Gould, D.B., Pearce, W., Carlsson, P., Enerback, S., Morissette, J., Bhattacharya, S., Hogan, B., Raymond, V., Walter, M.A., 1998. Mutations of the forkhead/winged-helix gene, *FKHL7*, in patients with Axenfeld–Rieger anomaly. Am. J. Hum. Genet. 63, 1316–1328.
Molina, G.A., Watkins, S.C., Tsang, M., 2007. Generation of FGF reporter transgenic zebrafish and their utility in chemical screens. BMC Dev. Biol. 7, 62.
Molotkov, A., Molotkova, N., Duester, G., 2006. Retinoic acid guides eye morphogenetic movements via paracrine signaling but is unnecessary for retinal dorsoventral patterning. Development 133, 1901–1910.
Nasevicius, A., Ekker, S.C., 2000. Effective targeted gene 'knockdown' in zebrafish. Nat. Genet. 26, 216–220.
Nishimura, D.Y., Swiderski, R.E., Alward, W.L., Searby, C.C., Patil, S.R., Bennet, S.R., Kanis, A.B., Gastier, J.M., Stone, E.M., Sheffield, V.C., 1998. The forkhead transcription factor gene *FKHL7* is responsible for glaucoma phenotypes which map to 6p25. Nat. Genet. 19, 140–147.
O'Hara, F.P., Beck, E., Barr, L.K., Wong, L.L., Kessler, D.S., Riddle, R.D., 2005. Zebrafish Lmx1b.1 and Lmx1b.2 are required for maintenance of the isthmic organizer. Development 132, 3163–3173.
Picker, A., Brand, M., 2005. Fgf signals from a novel signaling center determine axial patterning of the prospective neural retina. Development 132, 4951–4962.
Pressman, C.L., Chen, H., Johnson, R.L., 2000. LMX1B, a LIM homeodomain class transcription factor, is necessary for normal development of multiple tissues in the anterior segment of the murine eye. Genesis 26, 15–25.
Raible, F., Brand, M., 2001. Tight transcriptional control of the ETS domain factors Erm and Pea3 by Fgf signaling during early zebrafish development. Mech. Dev. 107, 105–117.
Reifers, F., Bohli, H., Walsh, E.C., Crossley, P.H., Stainier, D.Y., Brand, M., 1998. Fgf8 is mutated in zebrafish acerebellar (ace) mutants and is required for maintenance of midbrain–hindbrain boundary development and somitogenesis. Development 125, 2381–2395.
Robu, M.E., Larson, J.D., Nasevicius, A., Beiraghi, S., Brenner, C., Farber, S.A., Ekker, S.C., 2007. p53 activation by knockdown technologies. PLoS Genet. 3, e78.
Roehl, H., Nusslein-Volhard, C., 2001. Zebrafish pea3 and erm are general targets of FGF8 signaling. Curr. Biol. 11, 503–507.
Semina, E.V., Reiter, R., Leysens, N.J., Alward, W.L., Small, K.W., Datson, N.A., Siegel-Bartelt, J., Bierke-Nelson, D., Bitoun, P., Zabel, B.U., et al., 1996. Cloning and characterization of a novel bicoid-related homeobox transcription factor gene, *RIEG*, involved in Rieger syndrome. Nat. Genet. 14, 392–399.
Shanmugalingam, S., Houart, C., Picker, A., Reifers, F., Macdonald, R., Barth, A., Griffin, K., Brand, M., Wilson, S.W., 2000. Ace/Fgf8 is required for forebrain commissure formation and patterning of the telencephalon. Development 127, 2549–2561.
Smith, R.S., Zabaleta, A., Kume, T., Savinova, O.V., Kidson, S.H., Martin, J.E., Nishimura, D.Y., Alward, W.L., Hogan, B.L., John, S.W., 2000. Haploinsufficiency of the transcription factors FOXC1 and FOXC2 results in aberrant ocular development. Hum. Mol. Genet. 9, 1021–1032.
Soules, K., Link, B., 2005. Morphogenesis of the anterior segment in the zebrafish eye. BMC Dev. Biol. 5, 12.
Take-uchi, M., Clarke, J.D., Wilson, S.W., 2003. Hedgehog signalling maintains the optic stalk–retinal interface through the regulation of *Vax* gene activity. Development 130, 955–968.
Tamimi, Y., Skarie, J.M., Footz, T., Berry, F.B., Link, B.A., Walter, M.A., 2006. FGF19 is a target for FOXC1 regulation in ciliary body-derived cells. Hum. Mol. Genet. 15, 3229–3240.
Thisse, B., and Thisse, C., (2004). High throughput expression analysis in zebrafish. ZFIN Direct Submission http://zfin.org.
Trainor, P.A., Tam, P.P., 1995. Cranial paraxial mesoderm and neural crest cells of the mouse embryo: co-distribution in the craniofacial mesenchyme but distinct segregation in branchial arches. Development 121, 2569–2582.
Tsang, M., Friesel, R., Kudoh, T., Dawid, I.B., 2002. Identification of Sef, a novel modulator of FGF signalling. Nat. Cell Biol. 4, 165–169.
Vollrath, D., Jaramillo-Babb, V.L., Clough, M.V., McIntosh, I., Scott, K.M., Lichter, P.R., Richards, J.E., 1998. Loss-of-function mutations in the LIM-homeodomain gene, *LMX1B*, in nail-patella syndrome. Hum. Mol. Genet. 7, 1091–1098.
Walter, M.A., 2003. PITs and FOXes in ocular genetics: the Cogan lecture. Invest. Ophthalmol. Vis. Sci. 44, 1402–1405.